Phase Transformation and Residual Stresses after Laser Surface Modification of Metastable Austenitic Stainless Steel

Mohammad Rezayat[1, a)], Joan Josep Roa Rovira [1,2, b)], Antonio Mateo García[1,2, c)]

Author Affiliations
[1] *Center for Structural Integrity, Micromechanics, and Reliability of Materials (CIEFMA)-Department of Materials Science and Engineering, Universitat Politècnica de Catalunya-BarcelonaTECH, 08019 Barcelona, Spain.*
[2] *Barcelona Research Center in Multiscale Science and Engineering, Politècnica de Catalunya-BarcelonaTECH, 08019 Barcelona, Spain.*

Author Emails
[a)] *Corresponding author: Mohammad.Rezayat@Upc.edu*
[b)] *Joan.Josep.Roa@Upc.edu*
[c)] Antonio.Manuel.Mateo@Upc.edu

Abstract. Laser surface modification treatments have been applied to samples of a metastable austenitic stainless steel AISI 301LN. The amount of residual stresses and the presence of induced α´-martensite phase on the surface and subsurface of the samples, as a consequence of laser modification, have been investigated in this study. X-ray diffraction has been used to measure these values, which is a non-destructive method. Laser modification has been applied as parallel lines at a distance of 40 μm, using a laser intensity of 4 A and scanning speeds of 1, 3, and 5 bits/ms, frequency had a constant value of 1000 Hz. The results of the phase analysis show an increase in the α´-martensite present in the surface modified by the laser and that the sample corresponding to the lowest laser speed has the highest martensite fraction. Also, high tensile residual stresses were generated, more pronounced for the lowest laser scanning speed.

INTRODUCTION

Metastable Austenitic Stainless Steels (MASS) have been extensively studied over many years as good candidates to be used in industrial applications when mechanical properties such as formability, toughness, and weldability are required, particularly for automotive applications [1]. MASS are characterized by having an austenitic (*face-centered cubic*, FCC) microstructure which is not thermodynamically stable at room temperature. Therefore, when plastically deformed, the austenitic phase (γ) experiences a martensitic transformation that can produce two different types of martensite: ε (*hexagonal close packed*, HCP) and α' (*body-centered cubic*, BCC). A recent study by Barriobero-Vila et al. [2] by using high-energy synchrotron X-ray diffraction has revealed the transformation sequence of ε and α' , and provided light on the role of ε during α' transformation in MASS, showing that the latter is triggered by the general activation of slip. Moreover, the difference in packing density between γ and α' provides a volume expansion of ~ 4% [3], inducing residual stresses that can enhance the mechanical properties in terms of hardness and fatigue behavior.

On the other hand, A. Javan was the first to propose the concept of the laser in 1959 at the Bell Telephone Laboratories [4]. Javan, in collaboration with W.R. Bennett, Jr. and D.R. Herriott invented the laser in 1960, and two years later laser-welding was first used in springs manufacturing industries [5]. Nowadays, the laser has multiple

applications: for removing material (cleaning, cutting, drilling, etc) [6,7], deposition processes (welding, cladding, 3D printing) [8,9], and improving surface properties (shock peening, texturing) [10].

The present investigation deals with the laser surface modification of an AISI 301LN MASS. Laser Surface Modification (LSM) is defined as the result of the high heat energy coming from a laser beam, which is focused to melt the metal surface and a portion of the underlying substrate through a few microns depth, followed then by a fast solidification, which typically occurs with a cooling rate up to 1010 K/s. This technique has been demonstrated to be efficient to form highly resistant gradient layers [11]. Also, laser surface melting offers significant potential for improvement in surface properties as a result of homogenization and/or refinement of the microstructure. For example, Pacquentin, etc. al [12] used LSM with an austenitic stainless steel grade AISI 304L to improve mechanical properties and also corrosion resistance. Balla et al. [13] performed LSM on a medical grade AISI 316L and concluded that this treatment is a potential option for stainless steel-based biomedical devices to improve biocompatibility and corrosion resistance.

In this context, the main goal of this research is to evaluate the influence of one of the laser parameters, i.e, the scanning speed, as a small contribution to understanding the interaction Laser/Material. In doing so, phase transformations and induced residual stresses due to LSM were quantified.

MATERIALS AND METHODS

The AISI 301LN stainless steel, corresponding to European standard EN 1.4318, was provided by Outokumpu (Finland) as 1.5 mm thick annealed sheets whose chemical composition is given in Table 1.

TABLE 1. Chemical composition of the studied AISI 301LN.

Elements	Cr	Ni	Mn	Si	N	Mo	C	Fe
Wt%	17.6	6.50	1.13	0.42	0.17	0.04	0.02	Bal.

Figure 1a shows the geometry of the samples of AISI 301LN as a target material on which all tests and studies have been performed. Prior to laser modification, these samples were sequentially polished until a mirror like surface, by using the following diamond suspensions: 30, 6, and 3 μm. Finally, they were chemo-mechanically polished by using a neutral suspension of alumina (20-45 nm of average particle size). The aspect of nine samples after the laser treatment can be seen in Figure 1b. The different LSM conditions produce a variety of surface tonalities, according to the oxides generated because all the treatments were carried out in the air, without any shielding gas. The determination of those oxides is out of the scope of this paper, nevertheless, a complete analysis using Raman spectroscopy is provided by Liu et al. [14].

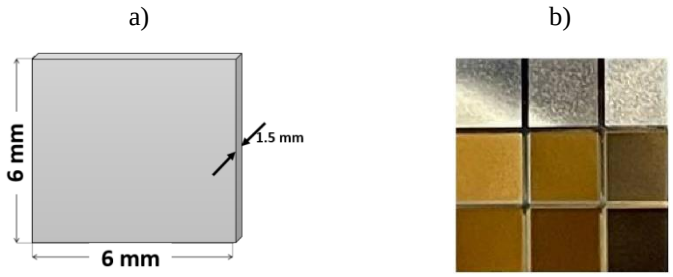

FIGURE 1. a) Schema of the sample with dimensions, b) Samples after laser surface modification (Silver color: low laser Intensity (2 A), and Golden color: high laser Intensity: (4 A).

X-ray diffraction (XRD) was employed to study the potential phase changes induced by the laser in the surface of the samples. The equipment used was a Bruker D8 Advance diffractometer whose characteristics are given in Table 2. The quantification of each phase was performed using the Reference Intensity Ratio (RIR) method [15].

TABLE 2. Condition of the X-ray Diffraction equipment.

Parameters	Step (°2Th.)	Cathode Wavelength (nm)	Start pos. (°2Th.)	End pos. (°2Th.)	Temperature (°C)
Amount	0.02	Copper (Cu) 0.154	3	120	25

Laser parameters

The laser equipment used for the surface treatments was an Explorer One 349-120 from Spectra-Physics. It is a nanosecond pulsed-beam solid-state laser Nd: YLF, with yttrium lithium fluoride crystals ($YLiF_4$) doped with neodymium ions (Nd^{+3}).

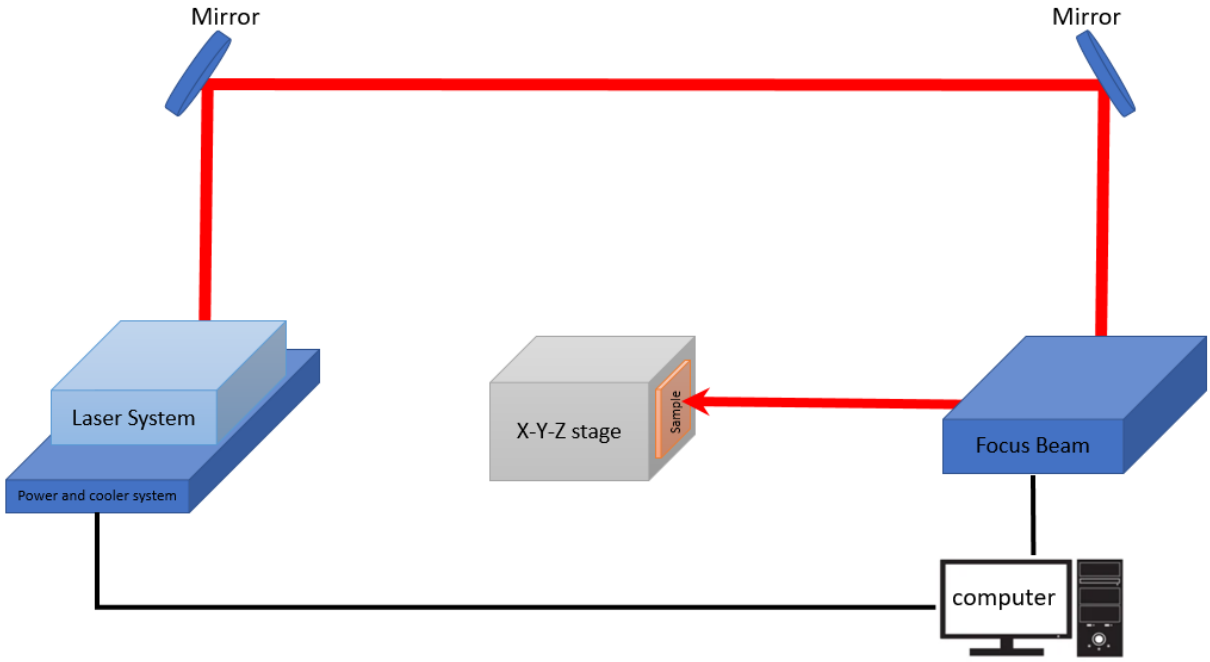

FIGURE 2. Schema of the laser equipment.

Figure 2 shows schematically the mechanism of this laser system. A laser beam is generated and two reflecting mirrors deviate this beam emitted up to convergent lenses that focalize it to the sample. The sample is fixed on a stage that allows positioning it along the three axes: X, Y, and Z. Table 3 gives the main characteristics of this laser equipment.

TABLE 3. Characteristics of the Explorer One 349-120 laser.

Wavelength (nm)	Pulse energy (µJ @1 kHz)	Output power (mW @1 kHz)	Pulse width (ns)	Beam diameter (mm)
349	120	120	< 5	0.16 ± 0.025

The above characteristics of the laser are fixed, but there are other parameters that can be modified by using the WeldMARK 3 software. They are Scanning speed (bit/ms), Intensity (A), Frequency (Hz), and also the design distance between laser lines (µm). Based on previous studies, for this research parallel lines with a distance between them constant and equal to 40 µm were applied, the intensity was always 4 A and the laser frequency was equal to 1000 Hz. Therefore, only the scanning speed was modified, with values of 1, 3, and 5 bits/ms. Accordingly, samples designation is S1, S3, and S5, respectively. The relationship between bits and micrometers is: 1 bit = 1.2 µm, so the applied

scanning speeds were: 1.2 mm/s for S1, 3.6 mm/s for S3, and 6 mm/s for S5. The laser patterns generated were observed by scanning electron microscope (SEM) in order to qualitatively characterize the induced topography.

Residual stresses measurement

The residual stress state in a component is the key factor of its behavior in service, particularly regarding high-strength materials and high applied loading. It is well-known that laser treatment can induce residual stresses on metal parts. For example, laser peening to provoke compressive residual stresses and then increase fatigue resistance is often applied to turbine engine blades [16]. Residual stresses can be due to various mechanisms, such as inelastic deformations, temperature gradients, and/or microstructural changes [17]. Almost all manufacturing processes, such as casting, welding, machining, plastic deformation during bending and rolling, etc., cause residual stress in the produced component [18]. While stresses from external loads can be measured with acceptable accuracy, it is not easy to predict residual stresses [19]. Therefore, it is important to have a reliable method to measure these stresses directly in a way that minimizes damage to the surface. In this research, residual stresses on the surface of the samples were measured at Saarland University (Germany) by X-ray diffraction using the 7-axis X-Ray Diffractometer PANalytical Empyrean. Measurements were done separately for each sample, employing Primary Side: Cr-tube, V filter, X-Ray Lens 1x1 mm, Secondary Side: Ray Lens 1x1 mm for α´-martensite, Secondary Side: Parallel Plate Collimator 0.27°, Proportional Detector, for the austenitic phase. The diameters of the points were 8 $\sin^2\Psi$. The peak middle positions were determined by the peak fit (center of gravity) method. Measured strain values were converted to stresses by Hooke's law assuming linear elastic and isotropic material behavior in this case 200-peak, $2\Theta°\sim79°$ [20,21]. The residual stresses diagram was drawn with normal stresses in two directions: σ_x-σ_y in Ψ 0° and 90°.

RESULTS AND DISCUSSION

Phase and topography evolution

Figure 3 shows the XRD diagrams for the material before LSM (As-Rec) and also for the three samples subjected to laser treatment, i.e., S5, S3, and S1.

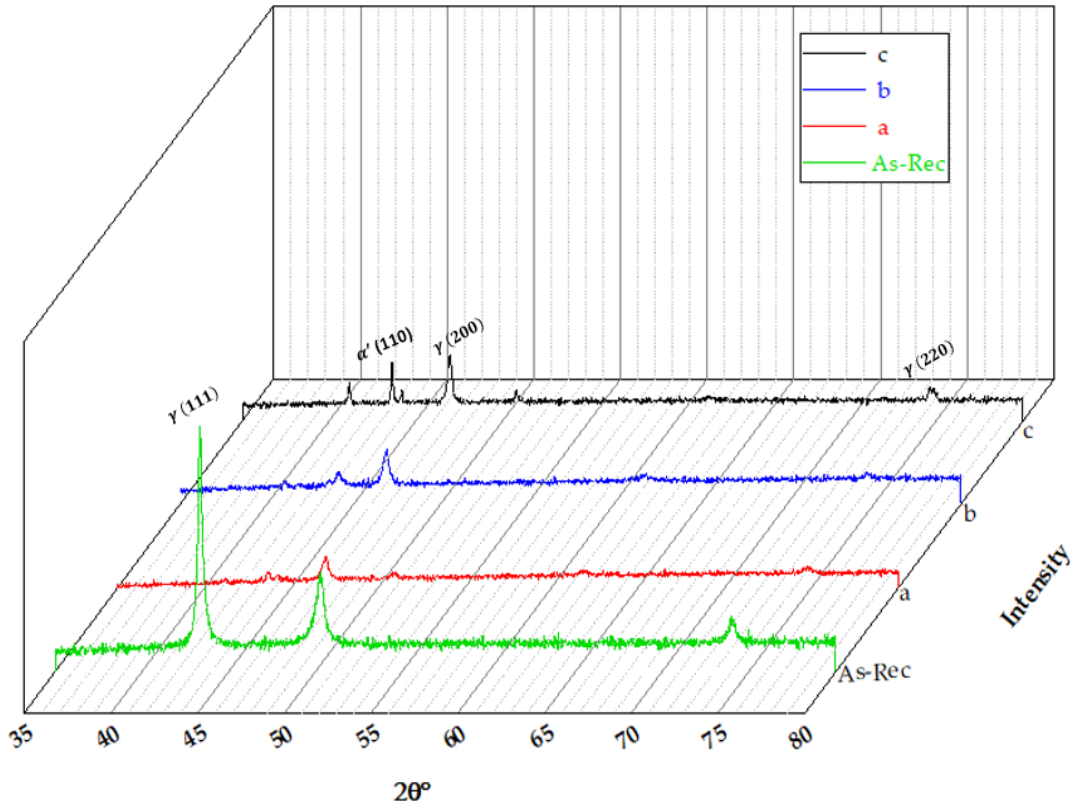

FIGURE 3. X-Ray diffraction diagram of four samples: As-Received, a) S5, b) S3, and c) S1.

In the reference sample, i.e, before LSM, the peaks found correspond to the austenite phase belonging to the following crystallographic planes: (111), (200), (220), (331), and (222). While for the martensite phase only one peak was found, whose crystallographic plane is (110). For samples after LSM, diffractograms showed several changes: peak corresponding to the austenitic plane (111) is much smaller and peaks related to martensitic phases, mainly (110), are marked. RIR quantification is indicated in Table 4.

TABLE 4. Austenitic and Martensitic phase quantification by Reference Intensity Ratio method (RIR).

Sample	**Reference**	**S1**	**S3**	**S5**
Austenite γ (%)	88.52	82.14	84.74	86.44
Martensite α′ (%)	11.48	17.86	15.26	13.56

The results from Table 4 point out that laser modification induces martensitic transformation. Moreover, the lowest scanning speed corresponds to a bigger increase of the martensite content 6 %, while the highest speed only produced 2 % of martensite.

After applying the laser to the surface of the samples, the surface melts, and then re-solidification occurs. Laser tracks are clearly distinguished in SEM images and even by naked eyes. Figure 4 collects SEM images showing that as the laser scanning speed decreases, the width of laser lines becomes larger because the beam will have the opportunity to melt more material. Lang et al. [22] explained the possible structuring mechanism by applying the Marangoni convection model for LSM. The mass transfer direction is dependent on the surface tension gradient of the melt pool. A combination of heat and mass transfer occurs in the melt pool at higher temperatures due to the lower

scanning speeds. Molten steel is separated and piled at the sides of the laser lines, as shown in Figure 5. This molten material causes ridges that protrude from the surface of the laser lines. In addition, the oxide layer on the surface of the sample S1, i.e, at the slowest laser speed, is more developed.

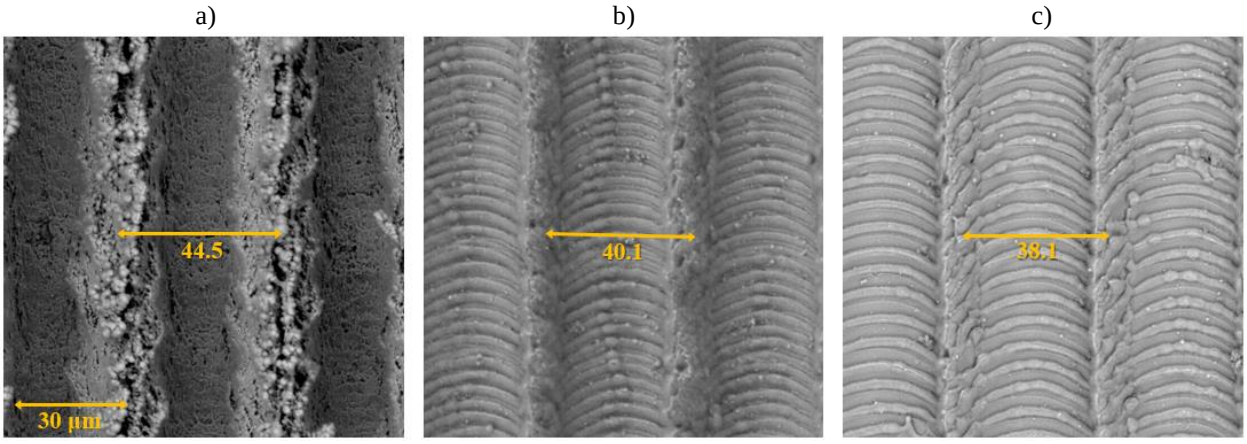

FIGURE 4. SEM images of the laser tracks corresponding to: a) S1, b)S3, c)S5

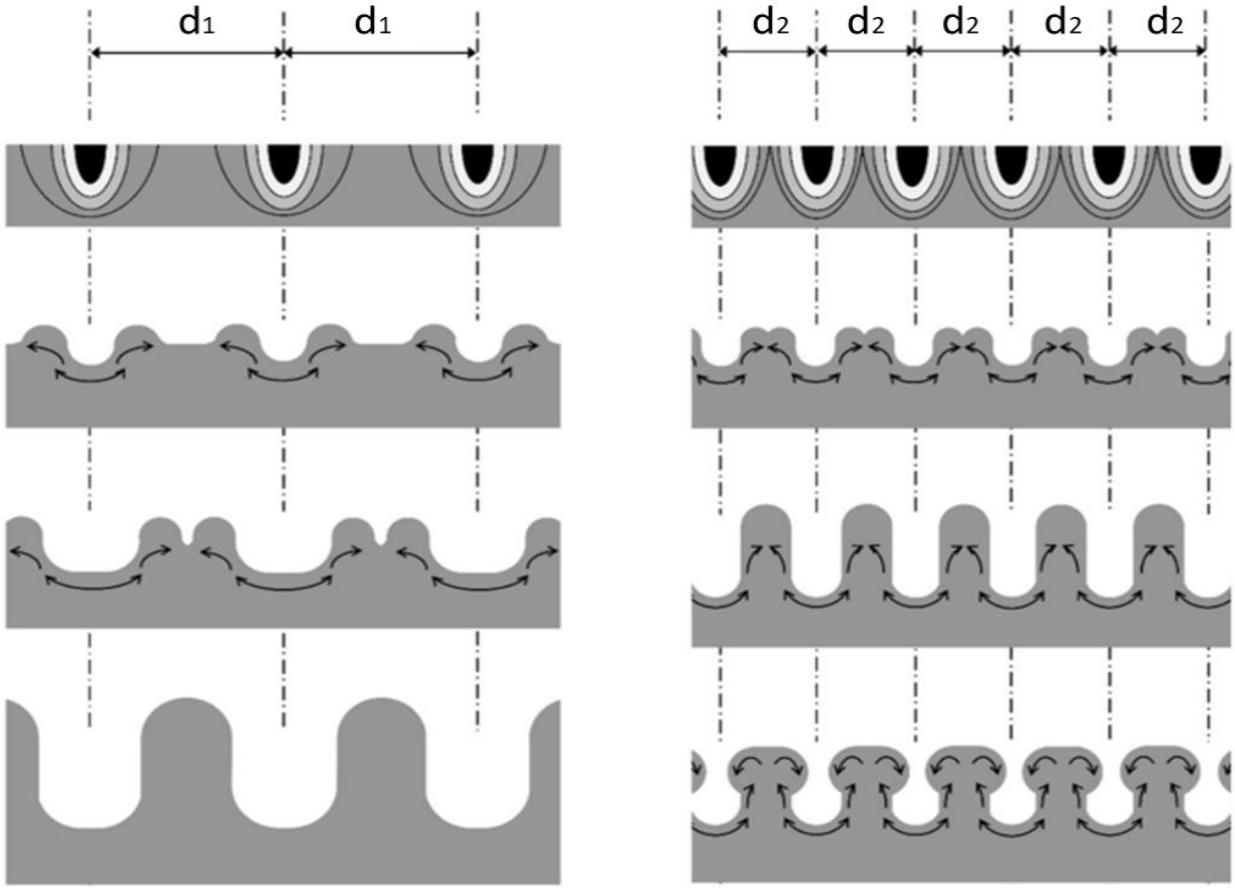

FIGURE 5. Mechanisms of the track formation by laser surface modification, depending of the distance between tracks [22].

Residual stresses

Residual stresses in AISI 301LN samples were calculated by the nanoscale X-ray diffraction method. This test is a non-destructive method, so in the case of very sensitive samples can be used to calculate and investigate the stresses at the surface and below the surface. This method is highly recommended for testing very small residual stresses [23,24]. On the other hand, comparing the values measured by the real residual stresses tests and those obtained from the computer simulation methods (FEM), it is concluded that the simulated values are very different from the real ones due to the usual unevenness of the surface of the sample and also to the limitations of measuring instruments [25]. In Figure 6, σ_x (longitudinal) and σ_y (transversal) directions of the residuals stresses are shown.

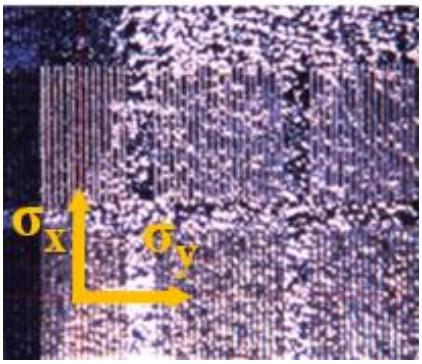

FIGURE 6. Optical image showing the laser patterns. The σ_x (longitudinal) and σ_y (transversal) overlapped to the image denote the direction of measurement of the residual stresses.

The d-spacing measurement as a function of $\sin 2\psi$ was obtained, as shown in Figure 7, and the calculations were performed to estimate the residual stress at the surface of the laser modified sample. It should be noted that the residual stress measured using the XRD technique provides the data in the surface region of the specimens [26]. Figure 8 shows that stresses in the X and Y directions are qualitatively similar, and by calculating these values, normal stresses can be obtained. As indicated in Figure 8, before LSM there are tensile stresses of around 350 MPa, which are attributed to the rolling and the annealing treatment given to the MASS. After the laser treatment, the magnitude of residual stresses increases and they reach very high values, even higher than the yield stress of the studied AISI 301LN, which is around 400 MPa. All of them are tensile and the lowest scanning speed induces the highest values of residual stresses, which agrees with the results reported in an AISI 420 martensitic stainless steel by Liu et al. [14]. Eigenmann et al. [27] explained that the resulting residual stresses are tensile as a consequence of the thermal contraction of the heated material during cooling mainly by self-quenching through heat transport into the interior of the samples. They also concluded that in the center of the track, stresses are slightly larger in longitudinal than in transverse direction, and demonstrated that after surface removal by electropolishing the tensile residual stresses decrease continuously with increasing distance from the surface. However, in the studied MASS the situation is more complex because another factor that can take a significant role is the potential transformation of austenite to martensite along the laser track, with the subsequent volume expansion. This fact could be the explanation of the higher residual stress values for the lowest laser speed, because for this condition the martensitic transformation was bigger. At the present, observations of the subsurface of the samples by performing FIB (Focus Ion Beam) milling, coupled with analysis with EBSD (Electron Back Scatter Diffraction) to locally distinguish austenite and martensite, are been carried out to study this aspect.

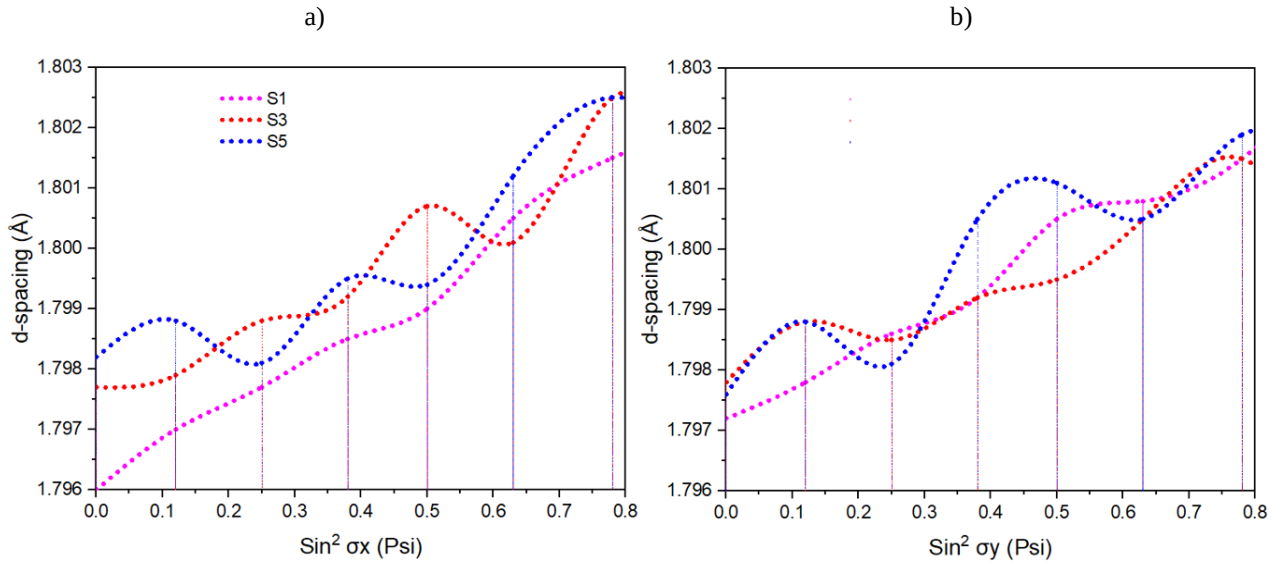

FIGURE 7. Residual stress diagram by using X-ray diffraction method. a) σ_x (longitudinal), and b) σ_y (transversal).

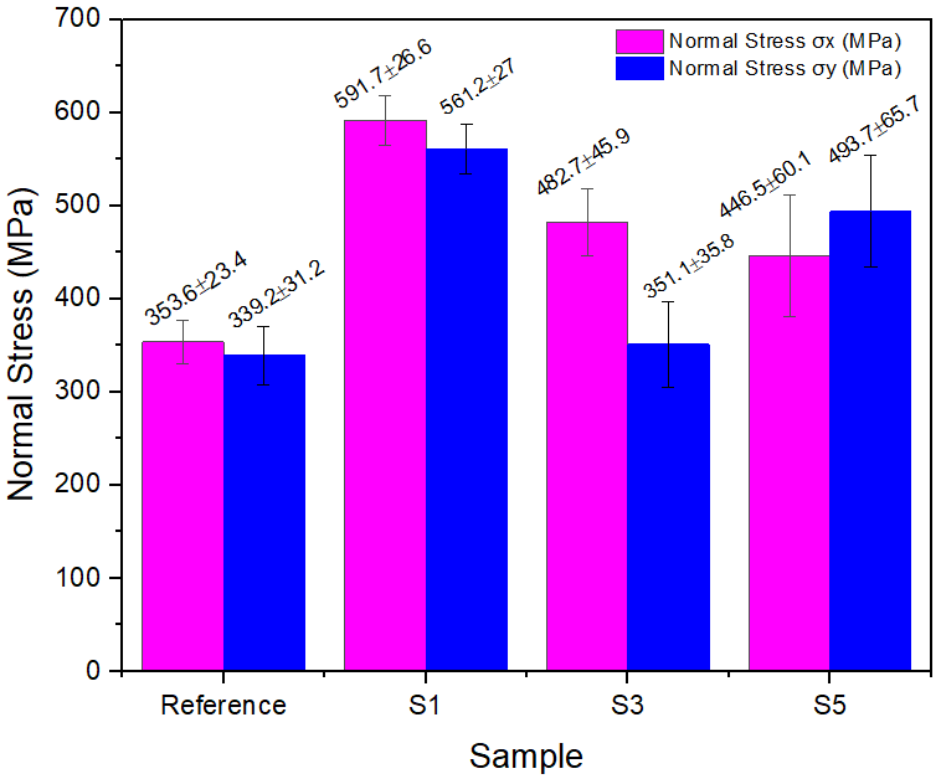

FIGURE 8. Residual stresses for the studied samples and the reference one.

CONCLUSIONS

According to the results obtained in the present study about laser surface modification of a metastable austenitic stainless steel, two main conclusions can be pointed out:

- Nanosecond pulsed-beam solid-state laser can be used for surface modification of stainless steel in the form of parallel laser tracks. This surface modification includes an increase of the martensitic phase at the surface and substrate of the metastable austenitic steel and the apparition of high tensile residual stresses.

- SEM images taken from the surface of the samples after the laser treatment show that the width of the laser tracks is directly related to the laser scanning speed, so as the speed decreases, the width of the laser lines increases.

- Low laser scanning speeds induce more martensitic transformation and higher residual stresses, probably as a consequence of the larger heat input.

ACKNOWLEDGMENTS

The authors would like to acknowledge Outokumpu for supplying the materials, and also the materials science department of Saarland University for helping with the residual stresses test. M. Rezayat acknowledges the AGAUR Programme of the Generalitat de Catalunya (FI-SDUR-2020) for financial support. The authors are also grateful to the Direcció General de Recerca del Comissionat per a Universitats I Recerca de la Generalitat de Catalunya for recognizing CIEFMA as a consolidated Research Group (2017SGR933).

REFERENCES

1. Y.H. Kim, K.Y. Kim, Y.D. Lee, Mater. Manufact. Proc. **19**, 51-59 (2004).
2. P. Barriobero-Vila *et al.*, Materialia **20**, 101251 (2021).
3. M. J. Santofimia, L. Zhao, and J. Sietsma, Mater. Sci. Forum, **706–709**, 2290–2295 (2012).
4. N. Taylor, *Laser : the inventor, the Nobel laureate, the thirty-year patent war* (Nick Taylor Simon Schuster, New York, 2000) pp. 184-216.
5. C. S. Willett and D. C. Lorents, Phys. Today, **29**, 71 (1976).
6. N. Levichev, G.C. Rodrigues, R. Dewil, J.R. Duflou, J. Laser Appl. **32**, 4505 (2020).
7. C.Y. Yap, C.K. Chua, Z.L. Dong, Z.H. Liu, D.Q. Zhang, L.E. Loh, S.L. Sing, Appl. Phys. Rev. **2**, 041101 (2015).
8. Z. Sun, X. Tan, S.B. Tor, C.K. Chua, NPG Asia Mater. **10,** 127–136 (2018).
9. M. Munther, T. Martin, A. Tajyar, L. Hackel, A. Beheshti, K. Davami, Engineering Research Express **2,** 34 (2020).
10. S. Martínez, A. Lamikiz, E. Ukar, A. Calleja, J.A. Arrizubieta, L.N. Lopez de Lacalle, Opt Laser. Eng. **90,** 72-80 (2017).
11. N. Jeyaprakash, IntechOpen **24**, 94439 (2021).
12. W. Pacquentin, N. Caron, and R. Oltra, Appl. Surf. Sci., **28,** 34–39 (2014).
13. V. K. Balla, S. Dey, A. A. Muthuchamy, G. D. Janaki Ram, M. Das, and A. Bandyopadhyay, J. Biomed. Mater. Res. B. Appl. Biomater., **106**, 2019-2028 (2018).
14. Q. Liu, M. Pang, J. Chen, G. Liu, and L. Zhang, Mater. Chem. Phys., **266,** 2000744 (2021).
15. Allison M. Beese, "Quantification of Phase Transformation in Stainless Steel 301LN Sheets, " Ph.D. thesis, Massachusetts Institute of Technology (MIT), 2008.
16. T. E. Pistochini and M. R. Hill, Fatigue Fract. Eng. Mater. Struct., **34,** 521-533 (2011).
17. Y. Peng, Z. Liu, Y. Jiang, B. Wang, J. Gong, and M. A. J. Somers, Scr. Mater., **157,** 100008 (2018).
18. Y. Zhan, Y. Li, E. Zhang, Y. Ge, and C. Liu, Appl. Acoust., **145,** 62-59 (2019).
19. R. M. N. Fleury, E. Salvati, D. Nowell, A. M. Korsunsky, F. Silva, and Y. H. Tai, Int. J. Fatigue, **119,** 34-42 (2019).

20. B. Mateša, Z. Kožuh, M. Dunđer, and I. Samardžić, Teh. Vjesn., **22,** 327-329 (2015).
21. B. Eigenmann, B. Scholtes, and E. Macherauch, Mater. Sci. Eng. A, **118**, 1-17 (1989).
22. V. Lang, B. Voisiat, T. Kunze, and A. F. Lasagni, Adv. Eng. Mater., **21** (2019)
23. A. S. Elmesalamy et al., Int. J. Press. Vessel. Pip., **147**, 64–78 (2016).
4. J. M. Alves, A. dos S. Paula, and L. P. Brandao, Mater. Res., **24**, 53-73 (2021).
25. L. Hartwig, J. Laser Micro/Nanoengineering, **5**, 128–133, (2010).
26. M. E. Fitzpatrick and A. Lodini, *Analysis of residual stress by diffraction using neutron and synchrotron radiation* (Taylor & Francis PP, London, 2003) pp.356-423.
27. B. Eigenmann, Transactions on Engineering Sciences **8**, , 10-24 (1995).